Model-based Climatology of Diurnal Variability in Stratospheric Ozone as a Data Analysis Tool

Stacey M. Frith[1], Pawan K. Bhartia[2], Luke D. Oman[2], Natalya A. Kramarova[2], Richard D. McPeters[2], Gordon J. Labow[1]

[1]Science Systems and Applications, Inc., Lanham, MD, USA
[2]NASA Goddard Space Flight Center, Greenbelt, MD, USA

Correspondence to: Stacey M. Frith (Stacey.Frith@nasa.gov)

Abstract. Observational studies of stratospheric ozone often involve data from multiple instruments that measure the ozone at different times of day. There has been an increased awareness of the potential impact of the diurnal cycle when interpreting measurements of stratospheric ozone at altitudes in the mid to upper stratosphere. To address this issue we present a climatological representation of diurnal variations in ozone with a half hour temporal resolution as a function of latitude, pressure and month, based on output from the NASA GEOS-GMI chemistry model run. This climatology can be applied in a wide range of ozone data analyses, including data inter-comparisons, data merging, and analysis of data from a single platform in a non-sun-synchronous orbit. We evaluate the diurnal climatology by comparing mean differences between ozone measurements made at different local solar times to the differences predicted by the diurnal model. The ozone diurnal cycle is a complicated function of latitude, pressure and season, with variations of less than 5% in the tropics and sub-tropics, increasing to more than 15% near the polar summer boundary in the upper stratosphere. These results compare well with previous modeling simulations and are supported by similar size variations in satellite observations. We present several example applications of the climatology in currently relevant data studies. We also compare this diurnal climatology to the diurnal signal from a previous iteration of the free-running GEOS Chemistry Climate Model (GEOSCCM) and to the ensemble runs of GEOS-GMI to test the sensitivity of the model diurnal cycle to changes in model formulation and simulated time period.

1 Introduction

Stratospheric ozone has been an environmental concern since the suggestion 45 years ago that anthropogenic chemicals (collectively known as ozone depleting substances; ODS) released into the atmosphere could destroy ozone [Stolarski and Cicerone, 1974; Molina and Roland, 1974]. Since that time, our understanding of ozone chemistry and dynamics has vastly evolved, and key to that evolution has been high quality satellite and ground-based observations of ozone. These observations were used to quantify ozone loss during the 1980s and early 1990s, and now are being used to quantify the turn around and expected increase in ozone after the ban of many ODS. However, the slow decline in these chemicals, resulting from their long atmospheric lifetimes and the staged reduction of their use through the Montreal Protocol and subsequent amendments, means that the ozone recovery rate will be much slower than the loss rate. Therefore observations must be sufficiently stable to resolve these small changes in time. Furthermore, measurements from more than one source are required to provide adequate spatial and time coverage to evaluate the full range of effects of ODS on ozone, such that data must be consistent across multiple observation platforms.

Inter-comparison of ozone observations from satellite and ground-based data sources is key to validating independent measurements and maintaining high quality data records. With the need for more stable long-term records, we must consider ever-smaller sources of variability. One such variation is the diurnal cycle in ozone, which had generally been considered small enough to be inconsequential in the middle stratosphere, though the large variations in the upper stratosphere and mesosphere are well known [e.g. Prather, 1981; Pallister and Tuck, 1983]. Although numerous studies have now highlighted observed and modeled peak to peak variations on the order of 5% or more in the middle stratosphere between 30 and 1 hPa [e.g., Sakazaki et al., 2013; Parrish et al., 2014; Schanz et al., 2014a and references therein], adequately resolving the signal on a global scale to account for its effects in data analysis is challenging. Ground-based microwave radiometers have been used to analyze the diurnal cycle in ozone at particular locations from the tropics to the northern hemisphere mid- and high-latitudes [i.e., Ricaud et al., 1991; Conner et al., 1994; Ogawa et al., 1996; Haefele et al., 2008; Palm et al., 2010; Parrish et al., 2014; Studer et al., 2014; Schranz et al., 2018]. Satellite data provides a more global view of the diurnal cycle. Several satellite missions, including the Upper Atmospheric Research Satellite (UARS) Microwave Limb

Sounder (MLS), the Superconducting Submillimeter-Wave Limb-Emission Sounder (SMILES), and the Sounding of the Atmosphere using Broadband Emission Radiometry (SABER) have made measurements from non-sun synchronous orbits that capture diurnal variations, but it takes more than a month to sample the full diurnal cycle, over which time the ozone has also undergone seasonal and other geophysical

5   changes. Thus, it takes averaging over many years or other statistical techniques to isolate the diurnal variations from other source of variability [e.g., Huang et al., 1997; Huang et al., 2010; Sakazaki et al., 2013]. These missions also do not provide full global coverage.

In this work, we present a climatology of diurnal variability as derived from the NASA Global Modeling and Assimilation Office (GMAO) Goddard Earth Observing System (GEOS) general circulation model

10   coupled to the NASA Global Modeling Initiative (GMI) chemistry package (GEOS-GMI) [e.g., Oman et al., 2013; Orbe et al., 2017]. The model-based climatology provides a global representation of the diurnal cycle as a function of latitude (5° zonal mean), pressure (~ 1 km equivalent altitude vertical resolution) and season (12 months). Parrish et al. [2014] compared the diurnal cycle in a version of this model to that measured by the microwave radiometer at Mauna Loa and found agreement within 1.5% in most cases

15   (see Parrish et al., 2014, Figures 8 and 9). Here we expand on those results, analyzing the model diurnal cycle against available measurements over a range of latitudes. As in the Parrish et al. study, most previous observational studies of the diurnal variability in ozone have included simulations from one or more models to support the observed differences, but we are not aware of a model-based climatology of the global diurnal cycle that is easily accessible for use in wide-ranging data applications. In this work

20   we do not focus on the chemical and dynamical mechanisms of the ozone diurnal cycle but rather on the validity of the model-derived diurnal climatology as a tool for data analysis. Hereafter we refer to the climatology as GDOC (GEOS-GMI Diurnal Ozone Climatology).

The paper is divided into the following sections: in section 2 we describe the model and the data used in this study; in section 3 we present GDOC and compare its variability to that observed by the SMILES

25   and the UARS and Aura MLS satellite instruments, as well to that from previously published observational and model-based studies; in section 4 we explore several example uses of GDOC in data analysis; and finally in section 5 we summarize our results, evaluate the robustness of the diurnal signal in multiple model runs, and detail how to access GDOC.

2 Data

2.1 GEOS-GMI Output and the Diurnal Ozone Climatology

The diurnal climatology presented in this work is based on output from the NASA GMAO Version 5 GEOS general circulation model, GEOS-5, [Molod et al., 2015] coupled with the NASA Global Modeling

5   Initiative (GMI) chemistry package [Strahan et al., 2007; Oman et al., 2013; Nielsen et al., 2017], known as GEOS-GMI. Unlike the GEOS Chemistry Climate Model (GEOSCCM) output used in Parrish et al. [2014], which was a free-running model, GEOS-GMI is run in replay mode [Orbe et al., 2017], with dynamics constrained by 3-hourly meteorological fields from the Modern Era Retrospective Analysis for Research and Applications, Version 2 (MERRA-2; Gelaro et al., 2017). The simulation, meant to be

10 concurrent with measurements from the Stratospheric Aerosol and Gas Experiment (SAGE) III instrument aboard the International Space Station (ISS), is currently available from 2017-2018, and will continue as input fields become available.

Model output are available every 30 minutes on a 1° by 1° latitude by longitude spatial grid. The model

15 is run on 72 pressure levels with a model top at .01 hPa, and output is interpolated to Z* pressure levels [pr=1013.25/10^(z/16.) hPa for z=0…80 km] with an approximate pressure-altitude vertical resolution of ~ 1 km (similar to the original model output). We construct the primary climatology by averaging two years of output (2017– 2018) as a function of latitude in 5° bins, pressure, month and time of day every 30 minutes. For each latitude, level and month, the hourly climatological values are normalized to the

20 value at midnight and the final climatology is expressed in terms of variation from midnight.

We also use output from the free-running GEOSCCM simulation as presented in Parrish et al. [2014] and from a previous iteration of GEOS-GMI to test the robustness of GDOC to changes in the model formulation (including updates to the input photochemistry and reaction rates) and to different simulation

25 years. Test climatologies from the additional model simulations are representative of different years but are constructed in the same manner. Supplemental Figure S10 shows an example of the diurnal climatologies constructed from four separate simulations. The overall patterns from all the simulations are very similar, suggesting the representation of the diurnal cycle within the model is well established.

2.2 Ozone Observations

We use ozone observations from multiple data sources to test GDOC in a variety of circumstances. Specifically, we use data from MLS instruments aboard the NASA UARS and Earth Observing Satellite

5 (EOS) Aura platforms; the second generation Solar Backscatter Ultraviolet (SBUV/2) series of instruments since 2000, which include those launched on NOAA satellites 16, 17, 18, and 19; the Ozone Monitoring Profiler Suite (OMPS) Limb Profiler (LP) and Nadir Profiler (NP) instruments aboard the NASA/NOAA Suomi National Polar-orbiting Partnership (S-NPP) satellite; the SMILES instrument which made measurements from the ISS and the SAGE III instrument currently aboard the ISS (hereafter

10 SAGE III/ISS). Table 1 shows the salient characteristics of the data sets used in this analysis and appropriate references for more information on each instrument.

All data records except SAGE III/ISS and OMPS LP are reported in pressure coordinates, and are first interpolated to Z* pressure levels. SAGE III/ISS and OMPS LP data are reported in altitude coordinates,

15 and MERRA-2 dynamical fields are used to convert between geometric altitude and pressure. Monthly climatological averages of satellite data are constructed (with the exception of SMILES and SAGE III/ISS, which are averaged over the entire available time period) in 5° latitude bins. UARS MLS and SMILES are additionally averaged into one-hour time bins. An estimated seasonal cycle is removed from the nine months of SMILES data as outlined in Sakazaki et al. [2013, Figure 3] and the data are not binned

20 by month. Though UARS MLS also samples the diurnal cycle over an extended period, the geophysical variability is largely removed in the 9-year average by month and the error bars capture the remaining variability. In this work we use UARS MLS data for qualitative comparisons only, and thus do not apply a more rigorous analysis to isolate the diurnal cycle.

3 Evaluation of Diurnal Climatology

3.1 Characterization of the Diurnal Cycle in GDOC

We first show several examples of GDOC, highlight some of the salient features, and compare generally to past studies. Figure 1 shows GDOC, normalized to the value at midnight, as a function of hour of day and pressure for four latitude bands and months. The ratio is shown with a contour interval of 0.025 (2.5%). The first panel (upper left) shows the climatology for March at 15-20° N. Here the most obvious feature is the low ozone during the day in the lower mesosphere, the well-known mesospheric ozone diurnal cycle [e.g. Pallister and Tuck, 1983]. There is very little if any variation in the nighttime values at these altitudes. Below 1 hPa there are variations at the sub-5% level. Unlike at higher levels, near 2 hPa the diurnal ozone nighttime values decrease by 2.5% between midnight and dawn, then vary up and down during the day (see also Figure 2). Results in this latitude band correspond to previous results shown in Parrish et al. [2014] comparing an earlier version of the model to diurnal variations derived from the microwave radiometer at Mauna Loa. Overall that study showed differences between model and data generally within 1-1.5%. The largest discrepancy was noted in the pre-dawn hours near 2 hPa, where the microwave instrument showed increasing rather than decreasing ozone. However data from the SMILES satellite also suggest the ozone is decreasing over this period (Figure 2; Parrish et al., Figure 10). Supplemental Figure S1 (top panels) show GDOC at 15-20° N for the additional months of January and June. The pre-dawn diurnal ozone decrease is larger in January, as was seen by Parrish et al.

The second panel (upper right) shows results for January at 45-50°N, which can be directly compared to a diurnal climatology developed from the GROMOS microwave radiometer in Bern, Switzerland [Studer et al., 2014, Figure 4a] as well as collocated model output from the Whole Atmosphere Community Climate Model (WACCM) and the Hamburg Model of Neutral and Ionized Atmosphere (HAMMONIA) used in the same study. Compared to the March subtropical climatology in the first panel, the shorter period of daylight hours is evident in the higher latitude January output. GDOC shows a loss of just over 20% at 0.3 hPa, which is somewhat less than that shown by GROMOS or the WACCM and HAMMONIA models, which are closer to 25%. Below about 1.5 hPa the pattern shifts from daytime low ozone to a pattern of lower ozone in the morning and higher ozone in the afternoon, with variations of greater than

5%. GROMOS and the collocated models show a similar shift, though at slightly different altitudes. GDOC agrees more closely with the model output from the GROMOS study, and the authors suggest the limited vertical resolution of the microwave data might be the cause of the discrepancy [Studer et al., 2014]. This characteristic pattern with higher afternoon ozone in the upper stratosphere diurnal cycle has

5 been widely reported in other observations from ground-based and satellite data [e.g., Haefele et al., 2008, Huang et al., 2008; Sakazaki et al., 2013, Parrish et al., 2014, Schranz et al., 2018]. Using the WACCM model, Schanz et al. [2014a] present a detailed breakdown of the photochemical reactions that contribute to the mid-latitude ozone diurnal cycle at 5 hPa (see also Haefele et al., 2008). Supplemental Figure S2 shows the seasonal variability of GDOC at 45-50°N at several altitudes, which matches the higher

10 amplitude diurnal cycle reported in summer by Studer et al. [2014] and Schanz et al. [2014a].

The lower two panels show the diurnal cycle in the northern hemisphere polar summer. The diurnal variability in both the mesosphere and stratosphere is largest near the Arctic Circle (lower left) and decreases nearer the pole (lower right). Near the polar day boundary, the diurnal cycle varies by greater

15 than 15% in the stratosphere. This large signal was reported in WACCM output by Schanz et al. [2014a; 2014b]. Recently, one year of microwave radiometer data taken at Ny-Alesund, Spitsbergen, Norway (79° N) showed similar variability with a June peak to peak variation of 5% at 1 hPa (night time ozone higher) and similar amplitude variations but with afternoon values higher at 3 hPa [Schranz et al., 2018]. The authors also included co-located WACCM model results in their analysis, which compared well with

20 the data after accounting for the reduced vertical resolution of the microwave instrument. The high-resolution WACCM output variations are 10% at 1 hPa and 8% at 3 hPa, in very close agreement with the GDOC signal at 75-80° S. Supplemental Figure S1 (bottom panels) shows the summer polar diurnal cycle in the Southern Hemisphere, which is nearly perfectly symmetric with that in the North.

25 Figure 2 shows GDOC at 65-70° N as a function of time of day at four pressure levels. Climatological values in March, June, September and December demonstrate the marked variation in the diurnal cycle with season at high latitudes. The summertime (June) diurnal cycle is the largest at all pressure levels. At 0.5 hPa the square-wave pattern dominates for all seasons, though it is weak in the winter. In the summer

the mesospheric diurnal pattern persists to 1 hPa, while other seasons show a more complicated pattern, with the equinox months showing a secondary peak in the late afternoon. At 3 and 5 hPa, all months except December show an early morning minimum and afternoon maximum. The December diurnal variability is confined to the hours around noon due to limited exposure to sunlight near the polar night boundary.

3.2 Diurnally-Resolved Satellite Data

In Figure 3, we directly compare the general features of GDOC at several pressure levels to those derived from diurnally resolved data from UARS MLS and SMILES satellite-based measurements as well as Aura MLS averages at 1:30am and 1:30pm (black symbols and vertical dotted lines). Specifically, we plot ozone variability as a function of hour of day normalized to the mean daily value for each product. Because of their orbital characteristics, both UARS MLS and SMILES have their best coverage within ~ 30° of the equator, so we limit our comparisons to low latitudes. We show results at 15-25°N in Figure 2, but other latitude bands in the tropics are similar. This comparison is qualitative in that we compare the zonal means and we do not attempt to isolate the diurnal cycle in the UARS MLS record beyond simply averaging the data over many years. The deseasonalized SMILES data as derived in Sakazaki et al. [2013] were provided by the authors [T. Sakazaki, personal communication, 2014]. Although the satellite data are noisy from hour to hour, the overall daily variability is accurately represented by GDOC. At 0.5 hPa the mesospheric diurnal pattern prevails, and GDOC captures the amplitude of the day to night ozone differences measured by the satellite data. At 1.5 hPa the pattern is a hybrid of the mesospheric and stratospheric diurnal cycle, with two relative maximums in the early morning and late afternoon, seen also in the SMILES data and to some degree by UARS MLS. Finally at 5 hPa the stratospheric pattern dominates, with measurements and climatology showing a relative high ozone value in the mid-afternoon. The satellite data agree within ~ 4% on the amplitude of the signal, with GDOC roughly reflecting the average of the satellite data.

3.3 Day Night Differences

We complete a more rigorous investigation of GDOC by analyzing the day-night differences in the model relative to the day-night differences in the Aura MLS record. At the equator Aura MLS makes measurements at 1:30 pm and 1:30 am local solar time, but at other latitudes the exact measurement time

5   varies due to the orbit inclination. Profiles from GDOC are selected to match the location and measurement local solar time of each MLS profile, and then averaged for direct comparison with MLS day and night averages. For this comparison when selecting the climatological profiles, we interpolate in time but not in latitude. Figure 4 shows the ratio of the daytime average to the nighttime average as measured by Aura MLS (top panels) and represented by corresponding profiles from GDOC (bottom

10   panels) as a function of latitude and pressure for two months, June and December.

The day to night ratio in the upper stratosphere, above ~ 1.5 hPa, shows the typical mesospheric diurnal pattern of low ozone in the daytime and high ozone at night [i.e., Pallister and Tuck, 1983]. Below this level the daytime ozone is higher than the nighttime value, but the pattern varies with latitude. As

15   expected, there is little variation between day and night values at high latitudes in polar night [see also Schranz et al., 2018]. In polar day, however, there is a variation of greater than 20% between 5 and 1 hPa near 70° N. Overall GDOC closely matches the spatial pattern and amplitude of that in the MLS with the ratios generally in agreement to within 2%. In the tropics near 1 hPa we note a local minima in the day to night ozone ratio in the Aura MLS data. GDOC also shows a local minima, but the amplitude of this

20   feature is not as pronounced as in the data. It is interesting to note the similarities in the pattern of the diurnal cycle below 30 hPa. However, we do not validate GDOC below 30 hPa because the diurnal variability is small and does not need to be accounted for at these levels.

Figure 5 shows profiles of the day to night ratio from the model and from Aura MLS at 65-70° N and 65-

25   70° S for the months of March, June, September and December. The error bars indicate twice the standard deviation of the Aura MLS profiles averaged from 2004-2018. Though there are some differences between the model simulations and observations, most notably the small shift in altitude in the June signal at 65-70° N and the offset above 2 hPa in September at 65-70° S, for the most part GDOC reliably

reproduces the signal in the observations within 2 percent or better. Additional profile comparisons of the day to night ratio from GDOC and Aura MLS can be found in Supplemental Figures S3-S8.

4 Example Diurnal Climatology Applications

4.1 SAGE III/ISS Sunrise Sunset Comparisons

5   SAGE III/ISS infers ozone profiles by measuring solar irradiance that has passed through the atmosphere during local sunrise and sunset events. One approach to evaluating these data is by checking the consistency of the measured sunrise and sunset profiles, but care must be taken to account for real diurnal differences between sunrise and sunset. Sakazaki et al. [2015] presented a thorough study of sunrise-sunset differences from occultation instruments SAGE II, UARS HALOE and ACE-FTS in the tropics

10   between 10° N and 10° S. Their analysis included output from the WACCM Specified Dynamics chemical transport model, and both observations and model indicated an asymmetry between sunrise and sunset measurements in the tropics, with sunrise satellite measurements being larger than those at sunset below ~30 km and above ~55 km. Figure 6 shows the estimated ratio of mean (2017-2018) SAGE III/ISS sunrise values to sunset values (SR/SS; red) and that computed from GDOC sub-sampled to match the

15   SAGE III/ISS measurements (blue). Results are shown in three broad latitude bands, and the SAGE III/ISS profiles have been interpolated to pressure levels in this comparison. Note that the spatial-temporal sampling of profiles is different in the sunrise and sunset averages. By matching the diurnal climatology to each profile we can represent the impact of the sampling on the diurnal cycle, but other geophysical variability may contribute to the measured differences. The SR/SS pattern from GDOC is similar to that

20   reported in Sakazaki et al. [2015] with sunrise profiles greater than sunset profiles (ratio > 1) below ~ 15 hPa (~ 30 km) and above ~ 0.7 hPa (~ 51 km) in the tropics (middle panel). We note that GDOC indicates SR/SS > 1 occurs at 51 km, which is somewhat lower than reported by Sakazaki et al. [2015] in observations (~55 km) and WACCM model results (~ 53 km). At middle latitudes, the GDOC sunrise/sunset differences are smaller (SR/SS is closer to 1), compared to the tropics, with little difference

25   below 15 hPa and a smaller difference in the upper stratosphere. The GDOC SR/SS pattern is also shifted downward by a few kilometers in the middle latitudes. The SAGE III/ISS SR/SS ratio generally follows

the pattern indicated by GDOC, and is within ~ 1% of the GDOC ratio below 2 hPa. Above 2 hPa GDOC and SAGE III/ISS diverge. At these levels the influence of the diurnal cycle on the SAGE III/ISS measurement is difficult to model because of the sharp diurnal gradient in the ozone along the line of site of the instrument. Also, as noted above, there is some variation between GDOC, WACCM and

5   observations in the SR/SS pattern in the tropics. Nevertheless these differences suggest potential discrepancies between SAGE III/ISS sunrise and sunset measurements that are currently being explored (R. Damadeo, personal communication, 2019). The purpose of this work is not to evaluate SAGE III/ISS observations but to demonstrate how GDOC can be used in such evaluations.

4.2 SAGE III/ISS Comparisons with Other Instruments

10   As with SAGE III/ISS internal sunrise/sunset comparisons, when evaluating the data relative to independent measurements, the local solar time of the measurements should be taken into account. Occultation instruments measure at local sunrise and sunset while limb and nadir measurements are taken at various times throughout the day, depending on the instrument (see Table 1). In this example we compare SAGE III/ISS sunrise and sunset profiles to co-located profiles from Aura MLS, OMPS Limb

15   Profiler (OMPS LP) and OMPS Nadir Profiler (OMPS NP). Both OMPS and Aura MLS measure at or near 1:30 pm local solar time. In the case of Aura MLS and OMPS LP, co-located profiles are defined as the nearest profile (within 1000 km) to the SAGE III/ISS profile, on the same day, and comparisons are done in altitude. For OMPS NP co-located profiles are the distance-weighted average of all profiles occurring within 1000 km of the SAGE profile on the same day and comparisons are on pressure levels.

20   Figure 7 show mean differences in the 20° - 60° N latitude band between SAGE III/ISS profiles (sunrise and sunset) relative to OMPS LP (upper panel) and Aura MLS (lower panel) before (red) and after (blue) using the diurnal climatology to 'adjust' the SAGE III/ISS profiles to the equivalent measurement time of the correlative data set. Again our intention is not to do a thorough analysis of the differences but to highlight the influence of the diurnal cycle when completing such analyses. Near 50 km, the mean

25   differences are reduced by 5% or more when accounting for the diurnal cycle. Similarly, differences are reduced below 44 km, with SAGE III/ISS coming into very good agreement with Aura MLS at these altitudes.

Figure 8 shows comparisons between SAGE III/ISS and OMPS NP profiles in three latitude bands. OMPS NP is a nadir backscatter measurement with a broad vertical resolution in the stratosphere. The SAGE III/ISS profiles are first integrated to match the OMPS NP vertical resolution before the sunrise and sunset profiles are averaged. The top panel shows the mean differences for sunrise-only (yellow) and sunset-only (purple) profiles. The bottom panel shows the same differences after the SAGE III/ISS profiles are converted using GDOC to an equivalent time of 1:30 pm to match the time of the OMPS NP measurements. Note that this comparison is focused lower in the stratosphere than in the previous figure. As such, the diurnal impacts are smaller. The largest changes are in the 1.0-1.6 and 1.6-2.5 hPa layers, though there are impacts at the 1-2% level in the 6-10 hPa layer and even lower in the tropics. After the diurnal adjustment, the sunrise and sunset biases are closer, and both indicate a shift in the bias above ~ 10 hPa. The remaining pattern of differences is consistent with the known bias pattern in the nadir UV backscatter series of instruments [i.e. Kramarova et al., 2013; Frith et al., 2017]. These examples illustrate how accounting for the diurnal cycle can help to both ascertain the true differences in the profiles and reduce noise in the inter-comparisons.

4.3 Merging SBUV Ozone Records

Representing the diurnal cycle is also important when merging multiple ozone data sets to construct a single long-term consistent data record. In this example we consider the SBUV series of nadir-view backscatter instruments, which is used to construct the Merged Ozone Data (MOD) record [Frith et al., 2014; Frith et al. 2017]. The SBUV/2 instruments on NOAA satellites were launched into drifting orbits such that the measurement time slowly changed over years. In addition, NOAA-17 SBUV/2 was launched into a late morning orbit, while the others were in early afternoon orbits, contributing to differences of several hours in overlapping measurements between instruments. Similarly, NOAA-16, though launched into an afternoon orbit, drifted such that measurements after 2012 were made in the early morning.

The combination of morning and afternoon orbits and drifting orbits can impart diurnally induced bias, drift and seasonal-scale variation between the SBUV/2 data records. We investigate this by comparing NOAA-16, -17 -18 and -19 to Aura MLS data from 2004-2017. Aura MLS profiles are integrated to match

the vertical sampling of the SBUV/2 data. Figure 9 shows the 4-6.4 hPa layer ozone difference time series at 10-15° S. The top panel shows the original differences between each SBUV/2 instrument and Aura MLS, and the bottom panel shows the differences after each SBUV measurement has been adjusted using GDOC to the Aura measurement time. Here the primary impact of the diurnal cycle correction is to reduce

5 the bias between the instruments. At the same latitude band but in the 2.5-4-hPa layer, shown in Figure 10, there are clear drifts over portions of the SBUV records relative to MLS that are largely removed after accounting for the diurnal cycle. Though in this case relative biases between the instruments remain, accounting for a consistent bias in a merged record is much easier than accounting for short-term drifts. Finally, Figure 11 shows the effect of the seasonal variation in the diurnal cycle at higher latitudes (see

10 Figure 4 and Figure S2). Here the SBUV instruments all show a seasonal cycle relative to Aura MLS, but after adjusting for the diurnal cycle the individual SBUV instrument seasonal cycles are in much better agreement relative to MLS. These varied effects can be understood by considering the diurnal cycle in each example, as shown in Supplemental Figure S9. The SBUV/2 records shown in Figures 9-11 vary in measurement time from 2 to 4 pm and from 8 to 10 am. At 10-15° S at 5 hPa there is a difference in the

15 diurnal cycle from morning to afternoon, but little change between 8 and 10 am or between 2 and 4 pm. However at 3 hPa there is a continuous gradient in ozone as a function of hour from 8 am to 4 pm. Thus, there is not only a bias between morning and afternoon measurements, but also a drift is induced as SBUV measurements shift earlier or later in time between the hours of 8 to 10 am and 2 to 4 pm. Finally, at 50-55°S at 7 hPa there is no diurnal signal in June-July-August but there is a 5% variation between morning

20 and afternoon ozone in December-January-February, leading to diurnally induced seasonal differences between instruments.

5 Summary and Conclusions

In this paper, we present a global climatology of the ozone diurnal cycle based on the NASA GEOS-GMI chemistry model. The climatology provides ozone levels every 30 minutes during the day, expressed as

25 the ratio of the value at midnight. It varies as a function of latitude, pressure, and month, with a latitude resolution of 5° and a vertical resolution of ~ 1 km equivalent pressure altitude. Previous studies of diurnal ozone observations often include co-located model results for comparison, but as far as the authors are

aware, this is the first easily accessible model-based climatology to be made available for general data analysis purposes. A model-based climatology is useful because no data source provides a full representation of the ozone diurnal cycle. However, this fact also makes the model output difficult to validate. Here we compare the climatology to time-resolved satellite-based data from UARS MLS and

5   SMILES, and compare the day to night climatological ratios to those derived from Aura MLS measurements. We also compare the climatology to previously published results including model analyses and diurnally resolved data from ground-based microwave radiometers. The GEOS-GMI diurnal climatology compares well with all sources; the most quantitative comparison against Aura MLS daytime to nighttime profiles ratios shows agreement typically within 2%.

The diurnal climatology depicts the largest variability during summer near the polar day boundary (65-70°), as reported previously by Schanz et al. [2014a, 2014b] based on WACCM model output. This is also supported by ratios of daytime to nighttime ozone profiles from Aura MLS. The hourly ozone variation transitions from a mesospheric pattern of low ozone during the day and high ozone at night to a

15   stratospheric pattern of low ozone in the morning and high ozone in the afternoon. However, the amplitude of the signals and the altitude of the transition vary significantly with season, leading to very complicated diurnal patterns that are not easily characterized in data inter-comparisons.

In this work we do not focus on the chemical and dynamical mechanisms of the diurnal cycle but rather

20   on the validity of the model-derived diurnal climatology as a tool for data analysis. We present a series of examples that highlight the usefulness of the climatology in data analysis as well as demonstrate the consistency between the observed and predicted ozone variations. In an additional test of the robustness of the diurnal cycle within the model, we considered several different simulations using iterative versions of the model and/or simulations of different years, and compared the diurnal cycle derived from each

25   simulation. Supplemental Figure S10 shows the December day-night ratios from diurnal climatologies constructed from four separate simulations. The overall patterns from all the simulations are very similar, suggesting the representation of the diurnal cycle within the model is well established.

Data Availability.

The GEOS-GMI diurnal ozone climatology is stored as a NetCDF file and is available for download on our local NASA Goddard Code 614 TOMS access site https://acd-ext.gsfc.nasa.gov/anonftp/toms/ (last

5 access August 20, 2019) under subdirectory GEOS-GMI_Diurnal_Climatology. Also available from this site are the SBUV/2 data (subdirectory sbuv) and OMPS NP data (subdirectory omps_np). These data are also accessible via links from the Merged Ozone Dataset (MOD) website at https://acd-ext.gsfc.nasa.gov/Data_services/merged/instruments.html (last access August 20, 2019). OMPS LP and NP data and UARS and Aura MLS data are archived at the NASA Goddard Earth Sciences Data and

10 Information Services Center (GES-DISC) (https://disc.gsfc.nasa.gov, last access August 20, 2019). SAGE III/ISS are available at the NASA Langley Atmospheric Science Data Center (ASDC) (https://eosweb.larc.nasa.gov/project/sageiii-iss/sageiii-iss_table, last access August 20, 2019). SMILES data are available from the Data Archives and Transmission System (DARTS) (http://darts.jaxa.jp/stp/smiles/, last access August 20, 2019). The Mauna Loa hourly resolved microwave

15 data are available by request (A. Parrish, parrish@astro.umass.edu). Additional model output from the current GEOS-GMI simulation is available for collaborators by request (L. D. Oman, luke.d.oman@nasa.gov).

Author Contributions.

20 S. M. Frith conducted the primary analysis including constructing the GEOS-GMI diurnal ozone climatology and applying the climatology to various data analysis tasks. L. D. Oman formulated and ran

the model simulations and provided guidance interpreting the model output. N. A. Kramarova provided

analysis of OMPS LP and SAGE III/ISS data. G. J. Labow contributed to Aura MLS and SBUV

measurement analysis. P.K. Bhartia conceived the original idea for this work and oversaw its

development, and R. D. McPeters provided funding support and project management. S. M. Frith prepared

5   the manuscript with significant contributions from all authors.

Competing Interests.

The authors declare that they have no conflict of interest.

10   *Acknowledgements.*

S. M. Frith is supported under NASA WBS 479717 (Long Term Measurement of Ozone). Model

simulations are supported by the SAGE III/ISS Science Team and NASA MAP programs and the high-

performance computing resources were provided by the NASA Center for Climate Simulation (NCCS).

The authors thank R. Stolarski for his helpful comments on the manuscript. We also thank the various

15   instrument teams for providing the data used in this study, particularly those responsible for SAGE

III/ISS, Aura MLS, OMPS and SBUV.

References

Bhartia, P. K., McPeters, R. D., Flynn, L. E., Taylor, S., Kramarova, N. A., Frith, S., Fisher, B., and
    DeLand, M.: Solar Backscatter UV (SBUV) total ozone and profile algorithm, Atmos. Meas. Tech., 6,
20   2533–2548, doi:10.5194/amt-6-2533-2013, 2013.
Chu, W. and Veiga, R.: SAGE III/EOS, Proc. SPIE, 3501, 52–60, doi:10.1117/12.577943, 1998.

Connor, B. J., Siskind, D. E., Tsou, J. J., Parrish, A., and Rems-berg, E. E.: Ground-based microwave observations of ozone in the upper stratosphere and mesosphere, J. Geophys. Res., 99, 16757–16770, doi:10.1029/94JD01153, 1994.

Frith, S. M., Stolarski, R. S., Kramarova, N. A., and McPeters, R. D.: Estimating uncertainties in the SBUV Version 8.6 merged profile ozone data set, Atmos. Chem. Phys., 17, 14695-14707, doi:10.5194/acp-17-14695-2017, 2017.

Frith, S. M., Kramarova, N. A., Stolarski, R. S., McPeters, R. D., Bhartia, P. K., and Labow, G. J.: Recent changes in total column ozone based on the SBUV Version 8.6 Merged Ozone Data Set, *J. Geophys. Res. Atmos.*, 119, 9735– 9751, doi:10.1002/2014JD021889, 2014.

Froidevaux, L., Jiang, Y. B., Lambert, A., Livesey, N. J.,Read, W. G., Waters, J. W., Browell, E. V., Hair, J. W., Avery, M. A., McGee, T. J., Twigg, L. W., Sumnicht, G. K.,Jucks, K. W., Margitan, J. J., Sen, B., Stachnik, R. A.,Toon, G. C., Bernath, P. F., Boone, C. D., Walker, K. A., Filipiak, M. J., Harwood, R. S., Fuller, R. A., Manney, G. L.,Schwartz, M. J., Daffer, W. H., Drouin, B. J., Cofield, R. E.,Cuddy, D. T., Jarnot, R. F., Knosp, B. W., Perun, V. S.,Snyder, W. V., Stek, P. C., Thurstans, R. P., and Wagner, P. A.: Validation of Aura Microwave Limb Sounder stratospheric ozone measurements, J. Geophys. Res., 113, D15S20, doi:10.1029/2007JD008771, 2008.

Gelaro, R., McCarty, W., Suárez, M. J., Todling, R., Molod, A., Takacs,L., Randles, C. A., Darmenov, A., Bosilovich, M. G., Reichle, R., Wargan, K., Coy, L., Cullather, R., Draper, C., Akella, S., Buchard, V., Conaty, A., da Silva, A. M., Gu, W., Kim, G., Koster, R., Lucchesi, R., Merkova, D., Nielsen, J. E., Partyka, G., Pawson, S., Putman, W., Rienecker, M., Schubert, S. D., Sienkiewicz, M., and Zhao, B.: The Modern-Era Retrospective Analysis for Research and Applications, Version 2 (MERRA-2). *J. Climate,* **30**, 5419–5454, doi:10.1175/JCLI-D-16-0758.1, 2017.

Haefele, A., Hocke, K., Kämpfer, N., Keckhut, P., Marchand, M.,Bekki, S., Morel, B., Egorova, T., and Rozanov, E.: Diurnal changes in middle atmospheric H2O and O3: observations in the Alpine region and climate models, J. Geophys. Res., 113, D17303, doi:10.1029/2008JD009892, 2008.

Huang, F. T., Reber, C. A., and Austin, J.: Ozone diurnal variations observed by UARS and their model simulation, J. Geophys. Res.,102, 12971–12985, doi:10.1029/97JD00461, 1997.

Huang, F.T., Mayr, H. G., Russell, J. M. I., and Mlynczak, M. G.: Ozone diurnal variations in the stratosphere and lower mesosphere, based on measurements from SABER on TIMED, J. Geophys. Res., 115, D24308, doi:10.1029/2010JD014484, 2010.

Kasai, Y., Sagawa, H., Kreyling, D., Dupuy, E., Baron, P., Mendrok, J., Suzuki, K., Sato, T. O.,
5   Nishibori, T., Mizobuchi, S., Kikuchi, K., Manabe, T., Ozeki, H., Sugita, T., Fujiwara, M., Irimajiri, Y., Walker, K. A., Bernath, P. F., Boone, C., Stiller, G., von Clarmann, T., Orphal, J., Urban, J., Murtagh, D., Llewellyn, E. J., Degenstein, D., Bourassa, A. E., Lloyd, N. D., Froidevaux, L., Birk, M., Wagner, G., Schreier, F., Xu, J., Vogt, P., Trautmann, T., and Yasui, M.: Validation of stratospheric and mesospheric ozone observed by SMILES from International Space Station, Atmos.
10   Meas. Tech., 6, 2311-2338, doi:10.5194/amt-6-2311-2013, 2013.

Kramarova, N. A., Frith, S. M., Bhartia, P. K., McPeters, R. D., Taylor, S. L., Fisher, B. L., Labow, G. J., and DeLand, M. T.: Validation of ozone monthly zonal mean profiles obtained from the version 8.6 Solar Backscatter Ultraviolet algorithm, Atmos. Chem. Phys., 13, 6887–6905, doi:10.5194/acp-13-6887-2013, 2013.

15 Kramarova, N. A., Bhartia, P. K., Jaross, G., Moy, L., Xu, P., Chen, Z., DeLand, M., Froidevaux, L., Livesey, N., Degenstein, D., Bourassa, A., Walker, K. A., and Sheese, P.: Validation of ozone profile retrievals derived from the OMPS LP version 2.5 algorithm against correlative satellite measurements, Atmos. Meas. Tech., 11, 2837-2861, doi:10.5194/amt-11-2837-2018, 2018.

Livesey, N. J., Read, W. G., Froidevaux, L., Waters, J. W., Santee, M. L., Pumphrey, H. C., Wu, D. L.,
20   Shippony, Z., and Jarnot, R. F.: The UARS Microwave Limb Sounder version 5 data set: Theory, characterization, and validation, J. Geophys. Res., 108, 4378, doi:10.1029/2002JD002273, D13, 2003.

McPeters, R. D., Bhartia, P. K., Haffner, D., Labow, G. J. and Flynn, L.: The version 8.6 SBUV ozone data record: An overview, J. Geophys. Res. Atmos., 118, 8032–8039, doi:10.1002/jgrd.50597, 2013.

McPeters, R., Frith, S., Kramarova, N., Ziemke, J., and Labow, G.: Trend quality ozone from NPP
25   OMPS: the version 2 processing, Atmos. Meas. Tech., 12, 977-985, doi:10.5194/amt-12-977-2019, 2019.

Molina, M. J., and Rowland, F. S.: Stratospheric sink for chlorofluoromethanes: Chlorine atomic catalysed destruction of ozone, Nature, 249, 810–812, doi:10.1038/249810a0, 1974.

Molod, A., Takacs, L., Suarez, M., and Bacmeister, J.: Development of the GEOS-5 atmospheric general circulation model: evolution from MERRA to MERRA2, Geosci. Model Dev., 8, 1339-1356, doi:10.5194/gmd-8-1339-2015, 2015.

Nielsen, J. E., Pawson, S., Molod, A., Auer, B., da Silva, A. M., Douglass, A. R., Duncan, B., Liang,
5   Q., Manyin, M., Oman, L. D., Putman, W., Strahan, S. E., and Wargan, K.: Chemical mechanisms and their applications in the Goddard Earth Observing System (GEOS) earth system model, J. Adv. Model. Earth Sy., 9, 3019–3044, doi:10.1002/2017MS001011, 2017.

Ogawa, H., Kawabata, K., Yonekura, Y., and Iwasaka, Y.: Diurnal and Seasonal Variations of Strato-Mesospheric Ozone, J. Geomag. Geoelectr., 49, 1115–1126, 1996.

10   Orbe, C., Oman, L. D., Strahan, S. E., Waugh, D. W., Pawson, S., Takacs, L. L., and Molod, A. M.: Large-scale atmospheric transport in GEOS replay simulations, *Journal of Advances in Modeling Earth Systems*, 9, 2545– 2560, doi:10.1002/2017MS001053, 2017.

Parrish, A., Boyd, I. S., Nedoluha, G. E., Bhartia, P. K., Frith, S. M., Kramarova, N. A., Connor, B. J., Bodeker, G. E., Froidevaux, L., Shiotani, M., and Sakazaki, T.: Diurnal variations of stratospheric
15   ozone measured by ground-based microwave remote sensing at the Mauna Loa NDACC site: measurement validation and GEOSCCM model comparison, Atmos. Chem. Phys., 14, 7255–7272, doi:10.5194/acp-14-7255-2 014, 2014.

Pallister, R. C., and Tuck, A. F.: The diurnal variation of ozone in the upper stratosphere as a test of photochemical theory, Q. J. R. Meteorol.Soc.,109, 271–284, 1983.

20   Palm, M., Hoffmann, C. G., Golchert, S. H. W., and Notholt, J.: The ground-based MW radiometer OZORAM on Spitsbergen – description and status of stratospheric and mesospheric O3-measurements, Atmos. Meas. Tech., 3, 1533–1545, doi:10.5194/amt-3-1533-2010, 2010.

Prather, M. J.: Ozone in the upper stratosphere and mesosphere, J. Geophys. Res., 86, 5325–5338, 1981.

Ricaud, P., Brillet, J., deLa Noë, J., Parisot, J. –P.: Diurnal and seasonal variations of stratomesospheric
25   ozone: Analysis of ground-based microwave measurements in Bordeaux, France, J. Geophys. Res., 96, 18,617–18,629, 1991.

Sakazaki, T., Shiotani, M., Suzuki, M., Kinnison, D., Zawodny, J. M., McHugh, M., and Walker, K. A.: Sunset–sunrise difference in solar occultation ozone measurements (SAGE II, HALOE, and ACE–

FTS) and its relationship to tidal vertical winds, Atmos. Chem. Phys., 15, 829-843, doi:10.5194/acp-15-829-2015, 2015.

Sakazaki, T., Fujiwara, M., Mitsuda, C., Imai, K., Manago, N.,Naito, Y., Nakamura, T., Akiyoshi, H., Kinnison, D., Sano, T.,Suzuki, M., and Shiotani, M.: Diurnal ozone variations in the stratosphere revealed

5 in observations from the Superconducting Submillimeter-Wave Limb-Emission Sounder (SMILES) onboard the International Space Station (ISS), J. Geophys. Res.-Atmos., 118, 2991–3006, doi:10.1002/jgrd.50220, 2013.

Schanz, A., Hocke, K., and Kämpfer, N.: Daily ozone cycle in the stratosphere: global, regional and seasonal behaviour modeled with the Whole Atmosphere Community Climate Model, Atmos. Chem.

10 Phys., 14, 7645–7663, doi:10.5194/acp-14-7645-2014, 2014a.

Schanz, A., Hocke, K., Kämpfer, N., Chabrillat, S., Inness, A., Palm, M., Notholt, J., Boyd, I., Parrish, A., and Kasai, Y.: The diurnal variation in stratospheric ozone from the MACC reanalysis, the ERA-Interim reanalysis, WACCM and Earth observation data: characteristics and intercomparison, Atmos. Chem. Phys. Discuss., 14, 32667–32708, doi:10.5194/acpd-14-32667-2014, 2014b.

15 Schranz, F., Fernandez, S., Kämpfer, N., and Palm, M.: Diurnal variation in middle-atmospheric ozone observed by ground-based microwave radiometry at Ny-Ålesund over 1 year, Atmos. Chem. Phys., 18, 4113-4130, doi:10.5194/acp-18-4113-2018, 2018.

Strahan, S. E., Duncan, B. N., and Hoor, P.: Observationally de-rived transport diagnostics for the lowermost stratosphere and their application to the GMI chemistry and transport model, Atmos.

20 Chem. Phys., 7, 2435–2445, doi:10.5194/acp-7-2435-2007, 2007.

Stolarski, R. S. and Cicerone, R. J.: Stratospheric chlorine: A possible sink for ozone, Canadian Journal of Chemistry, 52(8): 1610-1615, doi:10.1139/v74-233, 1974.

Studer, S., Hocke, K., Schanz, A., Schmidt, H., and Kämpfer, N.: A climatology of the diurnal variations in stratospheric and mesospheric ozone over Bern, Switzerland, Atmos. Chem. Phys.,

25 14,5905–5919, doi:10.5194/acp-14-5905-2014, 2014.

Table 1. Ozone Observations and Corresponding Measurement Times.

Instrument	Measurement Time at Equator	Period of Data (years)	Reference
Aura MLS (v4.2)	1:30pm; 1:30am	2004-2018	Froidevaux, 2008
SAGE III/ISS (aO3)	Local sunrise; Local sunset	2017-2018	Chu and Veiga, 1998
OMPS LP (v2.5) OMPS NP (v2.6)	1:30pm	2012-2018	LP: Kramarova et al., 2018 NP: McPeters et al., 2019
SBUV/2 (v8.6) ascending profiles NOAA-16, NOAA-18, NOAA-19	Orbit drifts slowly between 2pm and 4pm	NOAA-16: 2000-2007 NOAA-18: 2005-2012 NOAA-19: 2009-2018	McPeters et al., 2013 Bhartia et al., 2013
SBUV/2 (v8.6) descending profiles NOAA-16, NOAA-17	Orbit drifts slowly between 8am and 10am	NOAA-16: 2012-2014 NOAA-17: 2005-2011	McPeters et al., 2013 Bhartia et al., 2013
UARS MLS (v5)	Complete cycle 36 days	1991-1999	Livesay et al., 2003
SMILES (v2.4)	Complete cycle 30 days	Oct 2009-Apr 2010	Kasai et al., 2013
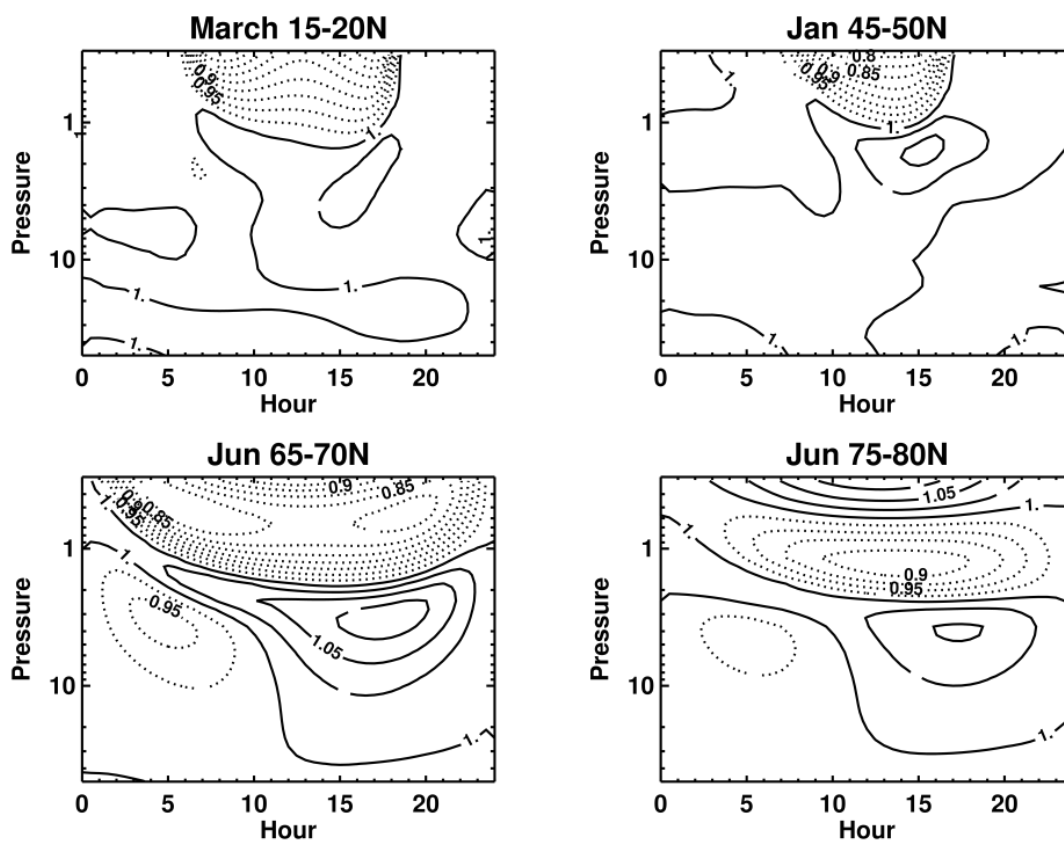
Figure 1. Contour plot of the GEOS-GMI diurnal ozone climatology (GDOC) normalized to the midnight value as a function of hour and pressure for March at 15-20° N (top left); January at 45-50° N (top right); June at 65-70° N (bottom left); and June at 75-80° N (bottom right). The contour interval is 0.025 (2.5%). The climatology is shown at levels from 30 hPa to 0.3 hPa.
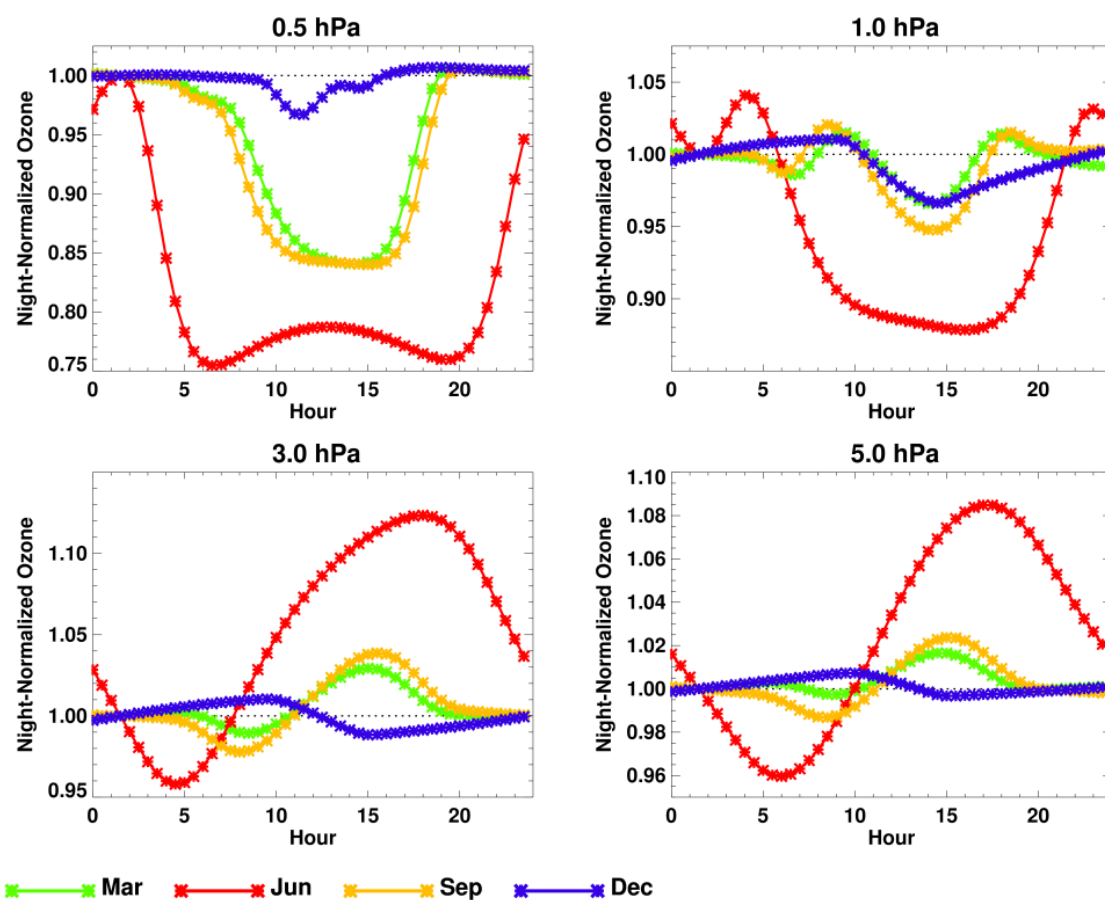
Figure 2. GDOC at 65-70° N as a function of season on four pressure levels: 0.5 hPa (top left); 1 hPa (top right); 3 hPa (bottom left); and 5 hPa (bottom right). Seasons are represented by monthly output in March, June, September and December. The diurnal signal is plotted as a function of hour (30-minute resolution) and is normalized to the 1:30am value.
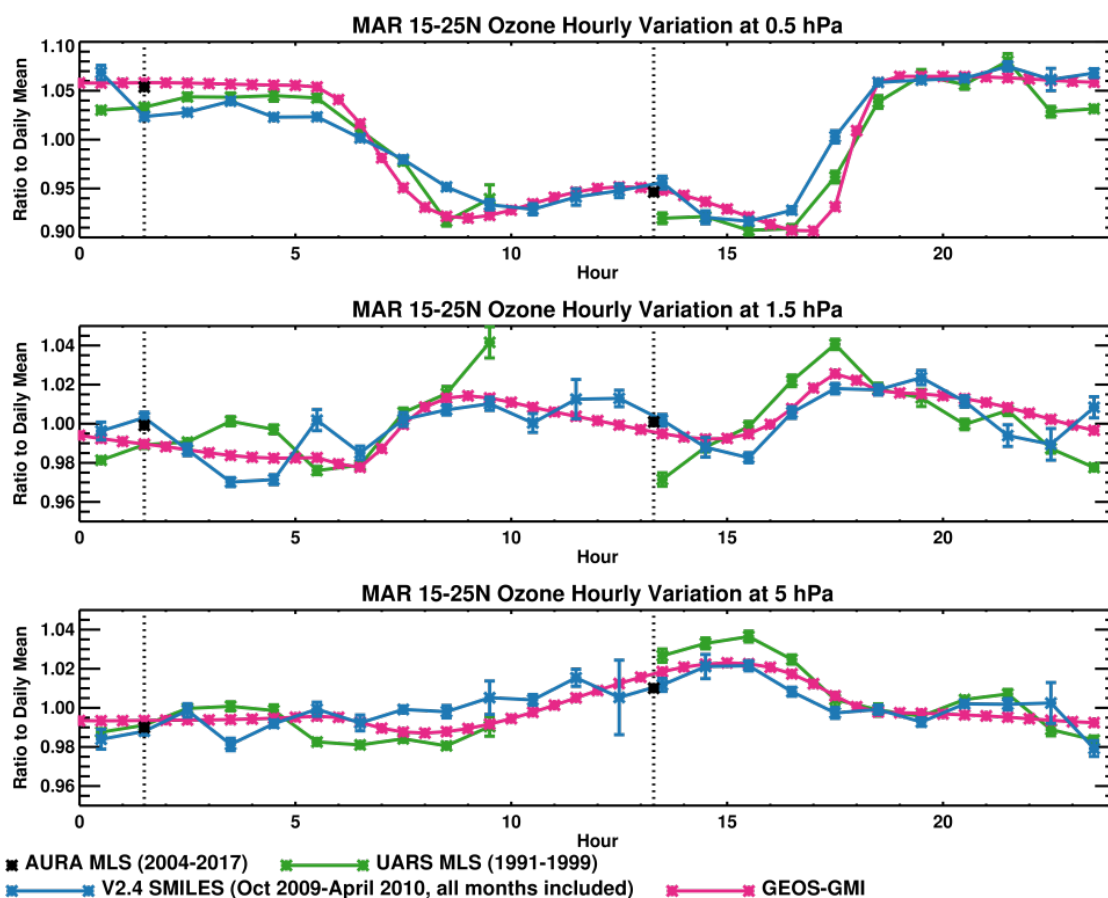
Figure 3. Diurnal variations as derived from SMILES (blue), UARS MLS (green) and Aura MLS (black symbols), compared to GDOC (red), plotted as a function of hour at three pressure levels: 0.5 hPa (top), 1.5 hPa (middle panel), and 5 hPa (bottom panel). Each product is normalized by its daily mean value, and the ratio is plotted. The black dotted lines indicate the two daily Aura MLS measurement times. UARS MLS means from 10am-1pm are not computed due to limited sampling.
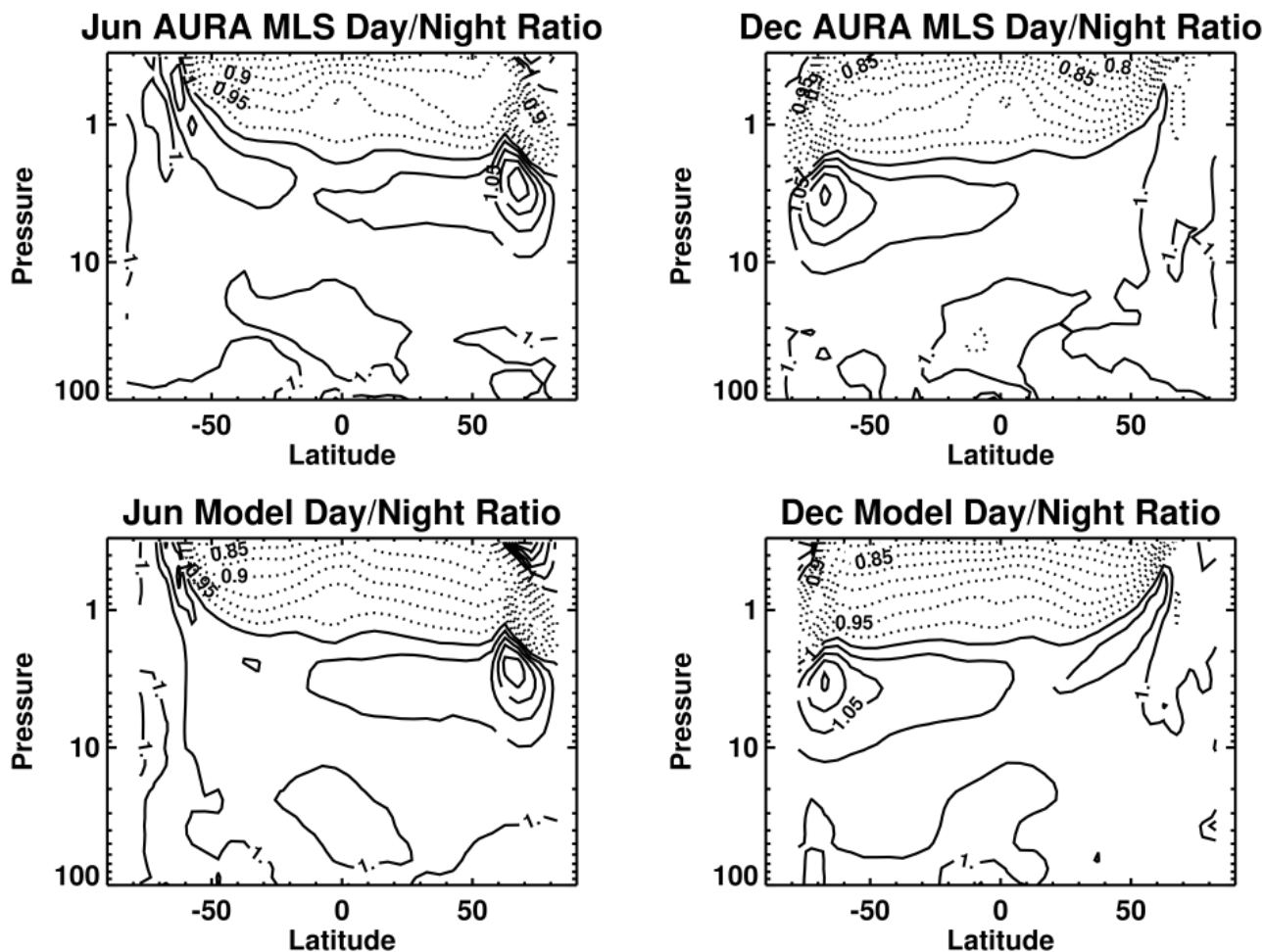
Figure 4. Aura MLS (top) and GDOC (bottom) ratio of day to night average ozone in June (left) and December (right) as a function of latitude and pressure from 100 hPa to 0.3 hPa. Contour interval is 0.025 (2.5%). GDOC is sampled at Aura MLS measurement times.
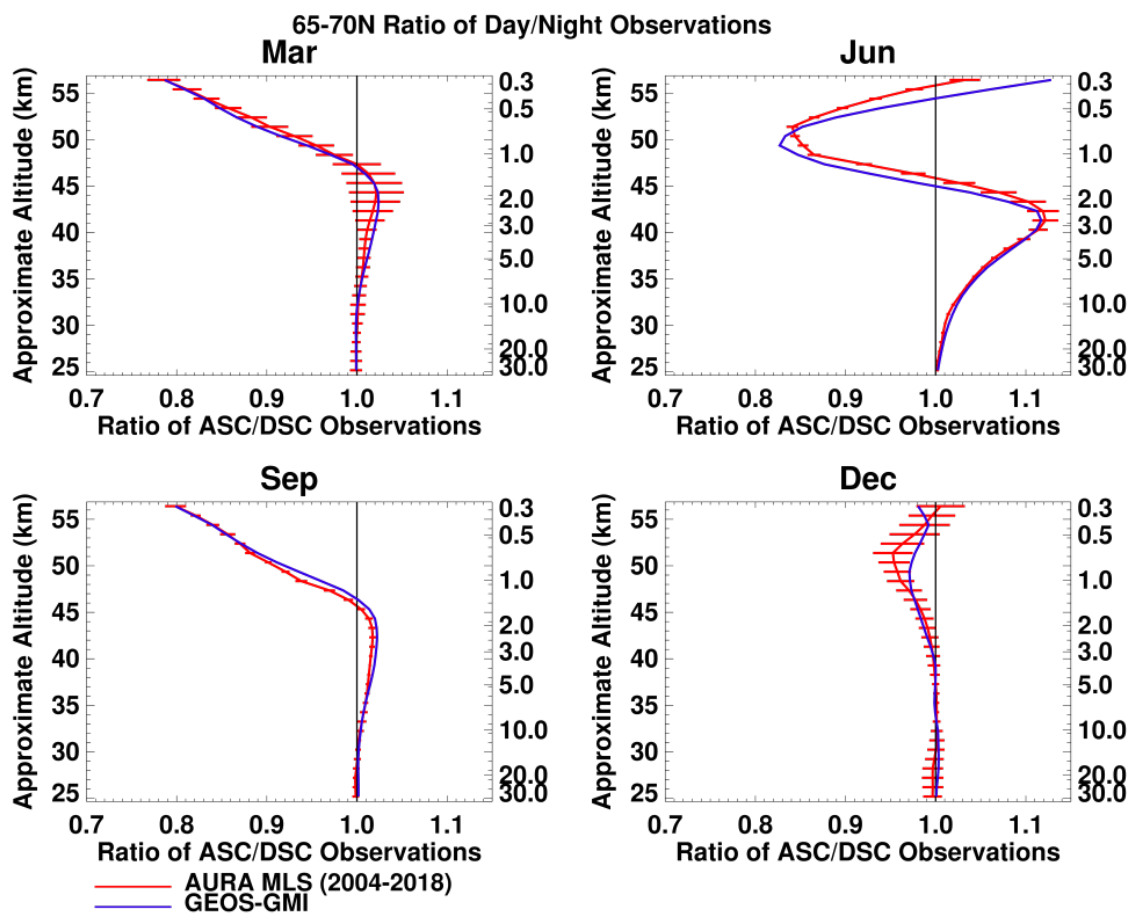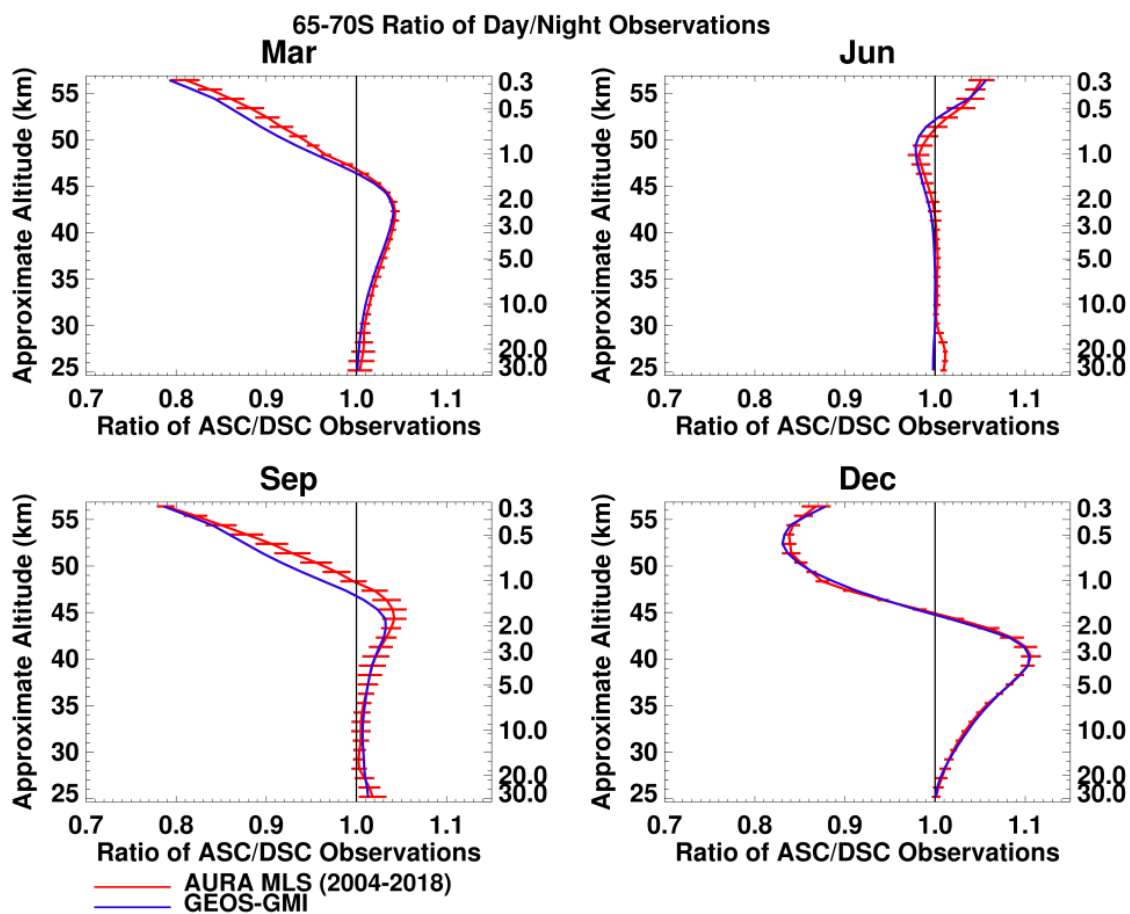
Figure 5. Profile of mean ratio of day to night measurements at 65-70° N (top four panels) and 65-70° S (bottom four panels) from Aura MLS (2004-2018) and GDOC sub-sampled at Aura MLS profile locations/times. Four panels show results for March, June, September and December. Error bars indicate the two-sigma standard deviation of Aura MLS day-night ratio profiles.
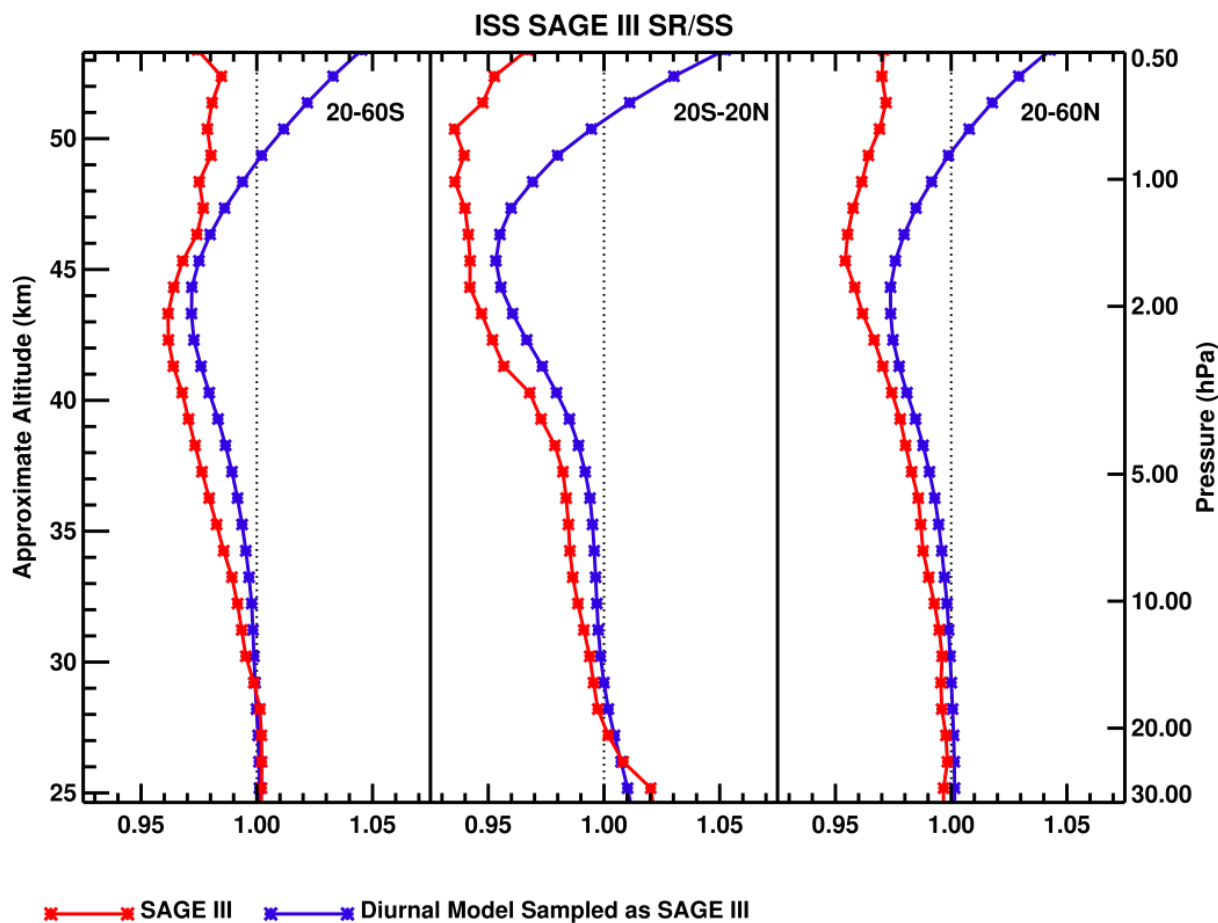
Figure 6. Ratio of mean sunrise to mean sunset ozone values from the SAGE III/ISS (red) and from GDOC (blue) sampled at SAGE III/ISS profile locations/times from 2017-2018. Ratios are shown averaged in broad latitude bands: 20-60° S (left); 20° S to 20° N (middle); and 20-60° N (right). Note that SAGE III measurements are such that the spatial and time sampling are different for the sunrise and sunset mean profiles.

SAGE III/ISS – OMPS LP   SAGE III/ISS-Aura MLS
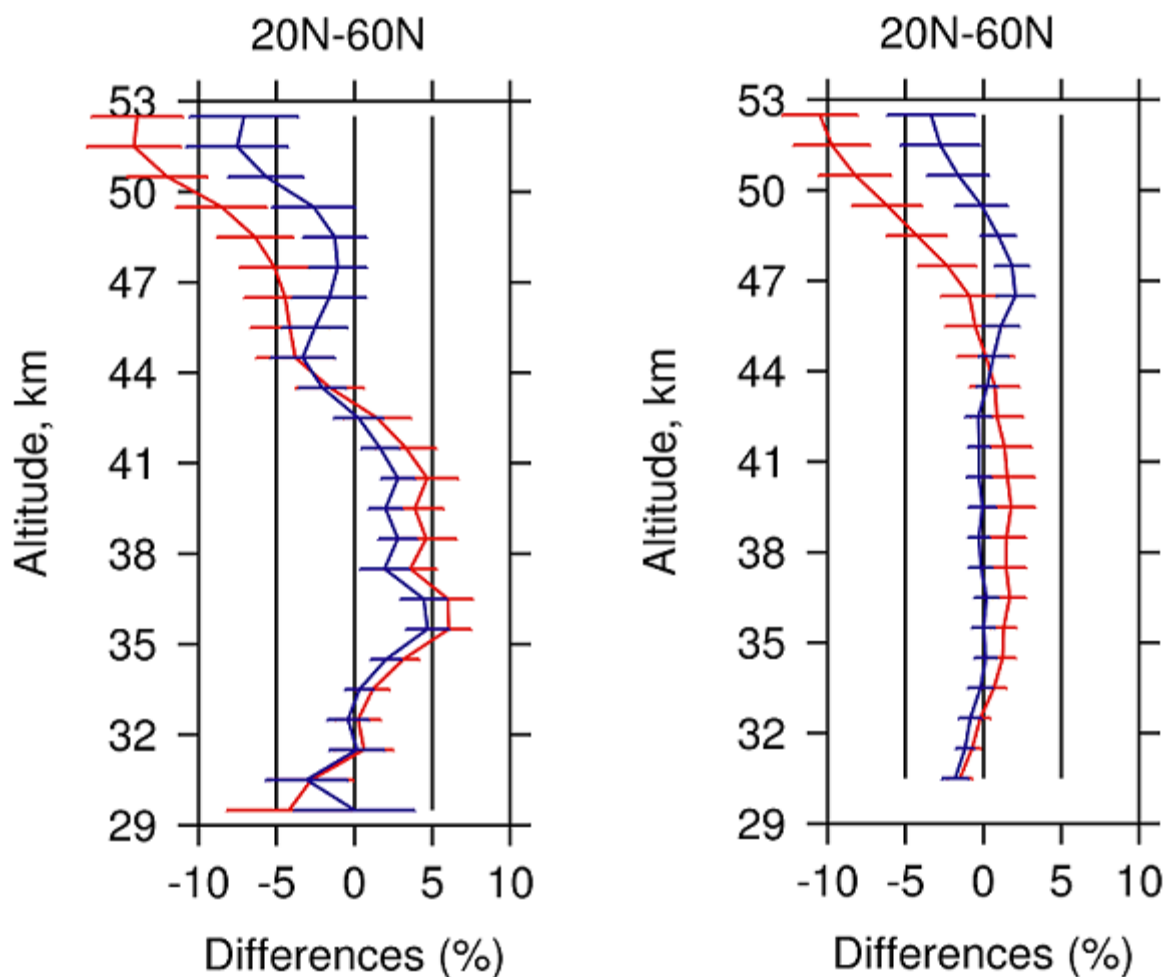
Figure 7. Profile of mean differences between SAGE III/ISS and OMPS Limb Profiler (left) and Aura MLS (right, daytime measurements only) averaged from 20° N to 60° N, expressed as percent difference as a function of altitude (km). Sunrise and sunset profiles are included in the mean difference. The red curve shows the original mean difference, while the blue curve shows the same comparison after using GDOC to adjust the SAGE profiles to an equivalent measurement time of 1:30pm to correspond to OMPS and Aura measurements.
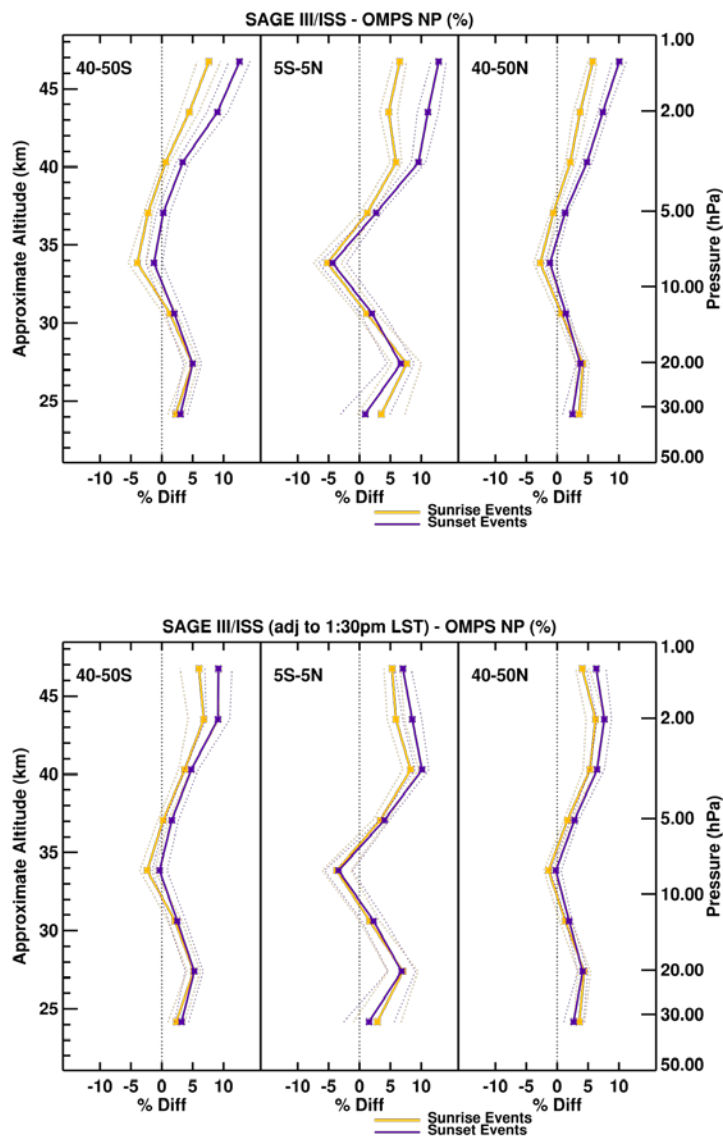
Figure 8. Profile of mean differences between SAGE III/ISS and OMPS Nadir Profiler (percent difference) as a function of pressure (hPa) separated by SAGE III/ISS sunrise and sunset profiles. Top panel shows original differences and bottom panel shows differences after the SAGE III/ISS profiles have been adjusted to the equivalent measurement time of the OMPS NP profiles.
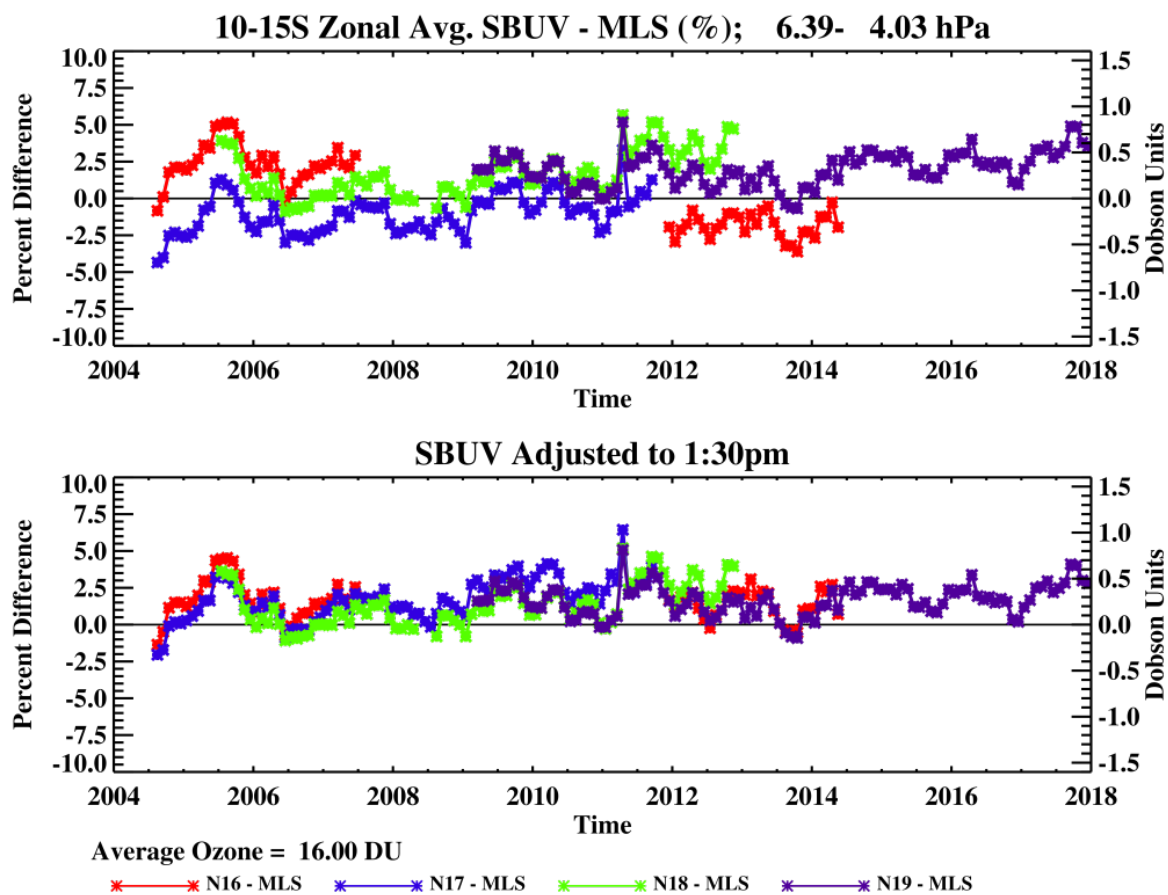
Figure 9. Time series of NOAA-16 through NOAA-19 SBUV zonal mean data relative to Aura MLS from 2004-2018 in the 10-15° S latitude band and 6-4 hPa pressure layer. Top panel shows original differences and bottom panel shows differences after individual SBUV instruments have been adjusted to common time of 1:30pm to coincide with Aura MLS measurement time.
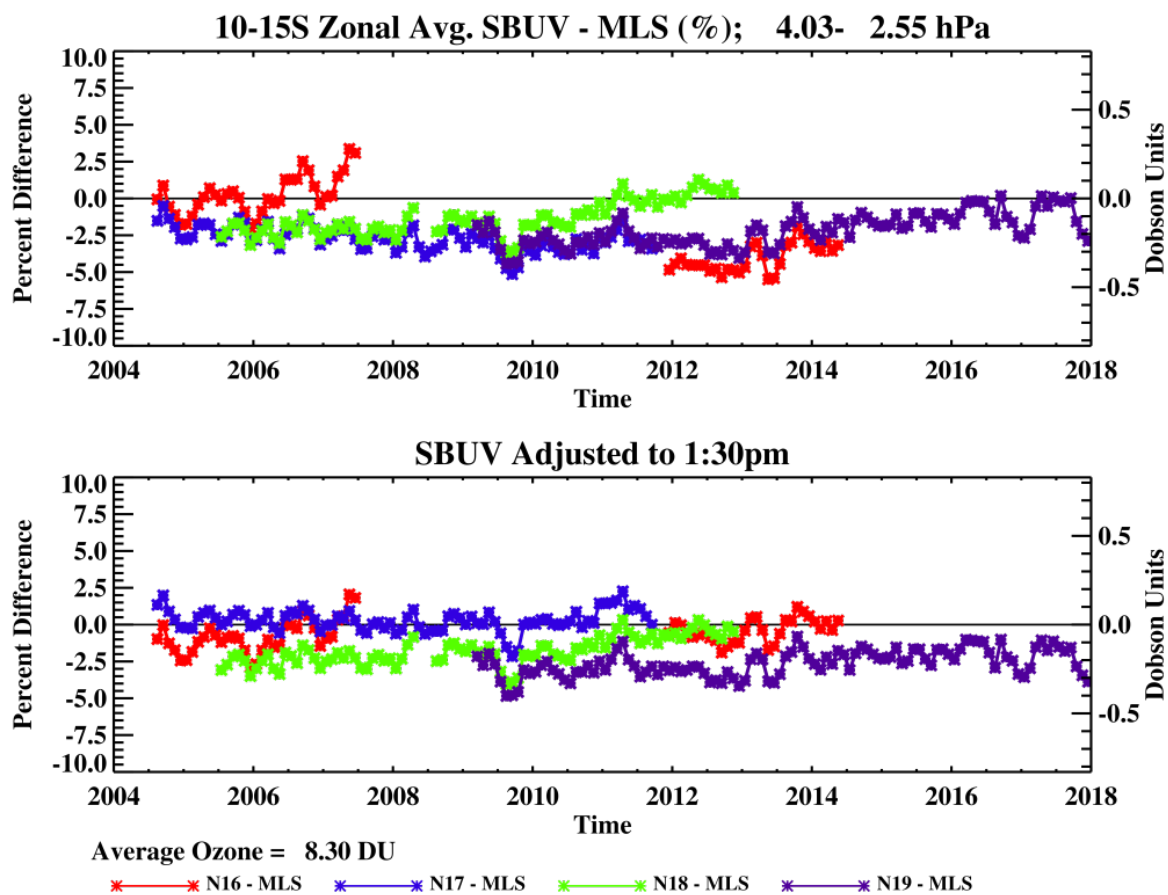
Figure 10. Same as Figure 10 but for 10-15° S latitude band at 4-2.5 hPa layer.
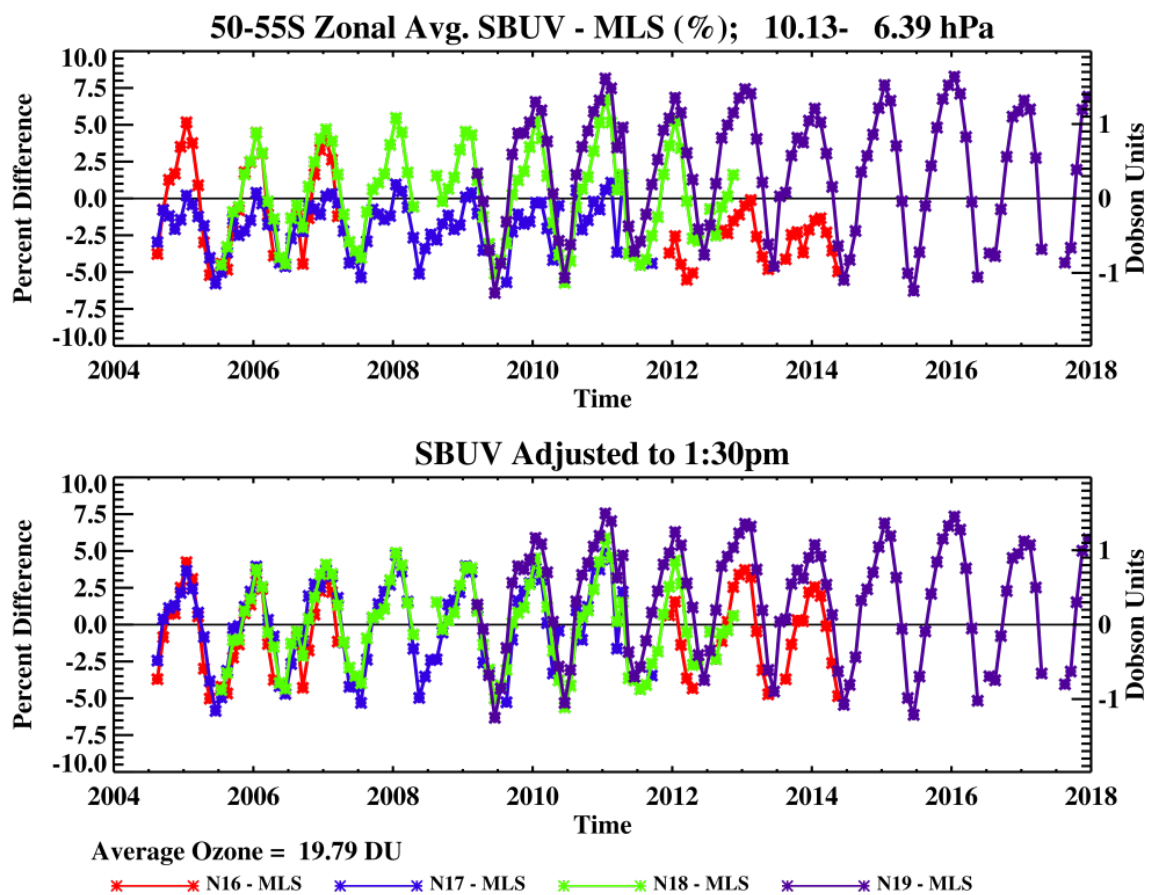
Figure 11. Same as Figure 10 but for 50-55° S latitude band at 10-6.4 hPa layer.